J Mater Sci (2009) 44:6363–6371
DOI 10.1007/s10853-009-3877-x

Erosion–corrosion behavior of plastic mold steel in solid/aqueous slurry

Dong-Cherng Wen

Received: 8 July 2009 / Accepted: 9 September 2009 / Published online: 23 September 2009

Abstract Erosion–corrosion behavior of a precipitation hardenable plastic mold steel (NAK80) has been investigated by using a rotated slurry erosion rig containing a slurry comprising 20 wt% Al_2O_3 particle and 3.5% NaCl solution. The erosion–corrosion rate and the synergism between erosion and corrosion have been determined under various conditions. The major environmental parameters considered are impact angle, impact velocity, and particle size. Post-test examination was conducted to identify the material degradation mechanism involved. The erosion–corrosion mechanisms of NAK80 mold steel at high-impact angles are dominated by the formation of impact pits, dissolution of metallic matrix, and plastic deformation fatigue spalling, whereas at low-impact angles, the mechanisms are dominated by the formation of impact pits, dissolution of metallic matrix, fatigue cracks, and cutting. The observed synergism between these mechanisms is much more accentuated at an oblique impact angle than that at a normal impact angle. At a given impact angle, the erosion–corrosion rate is found to increase with the impact velocity and the size of solid particles. The maximum peak of the erosion rates lies at oblique angles between 30° and 45°, whereas the maximum peak of the erosion–corrosion rates appears at 45°, and the erosion–corrosion rate is higher than the erosion rate alone at all angles examined. There is a positive synergism between erosion and corrosion for NAK80 mold steel in solid/aqueous slurry. The synergistic effect is 40–60% of the total weight loss. The contribution of synergism to the total weight loss depends upon the impact velocity; however, it is almost independent of the impact angle and particle size.

D.-C. Wen (✉)
Department of Mechanical Engineering, China University of Science and Technology, No. 245, Sec. 3, Academia Rd., Nangang District, Taipei City 11581, Taiwan, ROC
e-mail: dcwen@cc.chit.edu.tw

Introduction

The electronic and automotive industry is consistently increasing their production of polymer-based components. Applications are, for example, electronic connectors and bumpers in trucks and cars, especially those made of thermoplastics—usually polypropylene or reinforced ABS. In the injection molding of polymers, the mold is a critical element. Continuous growth in engineering plastics field necessitated the development of low-cost high-performance mold tool steels. Precipitation hardenable tool steels are now used for this application with good results—better quality, low costs, and improved performance. One example is NAK80 mold steel, a prehardened steel for fabricating plastic molds, which was developed by Daido Steel, Japan. This steel is usually supplied in the solution-treated condition, and its hardness ranges from 30 to 32 HRC. On aging at 500–530 °C for 5 h, the hardness ranges from 38 to 41 HRC [1]. With its excellent machinability, this steel is intended to replace AISI P-20 modified steel.

Wear and corrosion are the common problems in plastic injection molds, especially in high production molds. Erosion wear is induced by the reinforced resins flow and corrosion attack from acids and chloride formed by the decomposition of thermoplastic (e.g., PVC) due to overheating [2]. As a result of the combined effects of erosion and corrosion, the overall wear rate of material can be greater than the sum of the rates of material loss from either of the two processes, erosion and corrosion, acting separately. The additional part in material loss is defined in terms of synergistic effect [3–5].

Over the past several decades, there were a number of studies that reported synergistic effect of erosion and corrosion [6–12]. Many of these papers generally focused on the electrochemical behaviors such as electrode potential, corrosion current, and electrochemical corrosion rate [6–9]. Besides, extensive research has been done in understanding the pure erosion and corrosion mechanisms [13–16]. Also, some investigations reported the influence of experimental parameters on the corrosion of steels as well as studied the inhibition of corrosion [17, 18]. Although the problem caused by the interaction of erosion and corrosion is very serious, the mechanism of synergism is still not thoroughly understood because of its complexity. Clark and Hartwich [19] reported the effects of particle size on the erosion–corrosion behavior of 6061-T6 aluminum and Pyrex glass and concluded that there is generally a critical particle size. Below the critical particle size, the larger the particle size, the greater will be the weight loss. In contrast, beyond the critical particle size, erosion tends to achieve a steady state and does not increase any further again. Burstein and Sasaki [20] indicated that synergism effect between erosion and corrosion of 304 L stainless steel is enhanced by a more oblique angle of impact. Stack and Badia [21] constructed the erosion–corrosion maps of WC/Co–Cr-based composite as a function of impact velocity and applied potential under aqueous conditions. Lopez et al. [22] studied the effect of particle velocity and impact angle on the corrosion–erosion of AISI 304 and AISI 402 stainless steels and found that degradation of AISI 304 stainless steel was mainly determined by the mechanical action of impacting particles, and degradation of AISI 402 stainless steel occurred essentially through chemical action. However, erosion–corrosion behavior and synergistic effect are essential for a deep understanding of prehardened plastic mold steels, but very little work has been done on these aspects.

The primary aim of this investigation is to study the interaction and synergism between erosion and corrosion of prehardened plastic mold steel. The synergism of erosion and corrosion is discussed in terms of impact angle, impact velocity, and particle size.

Experimental details

Material

Test specimens of dimensions 80 mm × 25 mm × 3 mm were fabricated from commercial grade NAK80 mold steel supplied by Daido Steel, Japan. The major chemical compositions determined by Leco GDS-750 glow-discharge optical emission spectroscope analysis were (in wt%) C 0.12, Si 0.26, Mn 1.43, Ni 3.18, Al 1.02, Cu 0.95, Mo 0.22, and Fe balance. The material was received in the solution-treated condition (900 °C for 30 min and air cooled), and it had been aged at 500 °C for 5 h and had a hardness of 40.7 HRC. The microstructures of this material consisted of bainite and martensite, as shown in Fig. 1. The study of microstructural modification during aging of stainless steel and their effects on the impact strength and corrosion behavior has been examined in the literature [23]. The results indicate that the corrosion resistance is less markedly affected by the precipitation of carbides and nitrides.

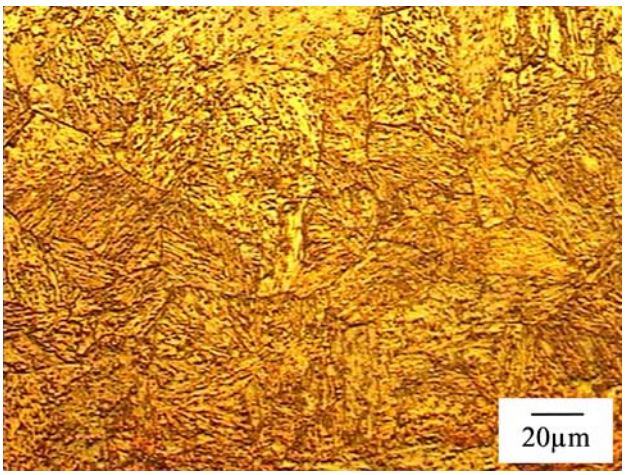

Fig. 1 Microstructure of NAK80 mold steel in the solubilized and aged state (Nital 4%)

Initial surface roughness is a critical parameter in determining the pitting potential of metals [24]; rougher surfaces of the same metal exhibit lower pitting potentials. To minimize the difference resulting from variation in roughness, each specimen was grounded by silicon carbide papers up to 1200 grid to 0.103 ± 0.023 μm R_a. After grounding, the specimen was washed in water, dipped in acetone, dried in warm air, and weighed by using an analytical balance with an accuracy of 0.1 mg. After the erosion–corrosion test, the specimen was removed and cleaned ultrasonically with alcohol for 15 min to eliminate the impact particles stuck on the surface for re-weighed and worn surface observation.

Corrosion test

EG&G Princeton Applied Research Potentiostat/Galvanostat Model 362A outfitted with analysis software CorrWare was used to evaluate electrochemical behavior. The flat cell is a three-electrode set-up consisting of the specimen as the working electrode, a saturated calomel electrode (SCE) as the reference electrode, and a platinum sheet used as the counter electrode. Potentiodynamic polarization was swept from −1000 to +1500 mV at a fixed rate of 1 mV/s. 3.5%

NaCl solution was used as the electrolyte. The obtained anodic polarization curve was used to calculate the pure corrosion rate (W_c).

Erosion–corrosion test

The erosion–corrosion test was carried out by using a rotating slurry wear tester as shown in Fig. 2a with the same electrolyte as that in corrosion test plus 20 wt% of irregular Al_2O_3 particles. The tester mainly consisted of a large plastic container, specimen holder, and a stirring blade. Four specimens were fixed on the specimen holder at the same time and soaked in slurry while testing. The rotation diameter of the specimens was 200 mm; the rotation speeds are 400, 700, and 1000 rpm and the corresponding linear velocities are 4.2, 7.3, and 10.4 m/s. The bolts fixed in the holder could adjust the specimens against impact angles of solid particles (Fig. 2b). The parameters for erosion–corrosion test are presented in Table 1. Additionally, these impinged particles and solution were never used more than once.

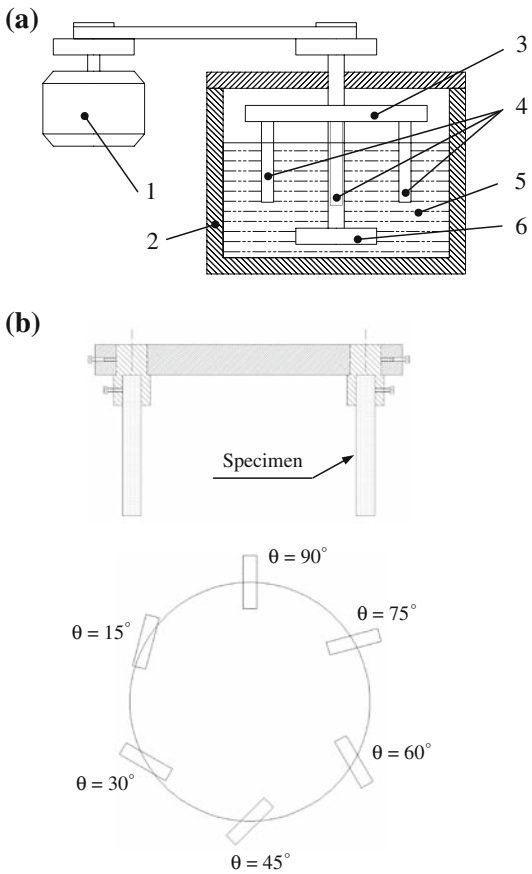

Fig. 2 **a** Schematic representation of the erosion–corrosion tester: (*1*) motor, (*2*) slurry pool, (*3*) specimen holder, (*4*) specimens, (*5*) slurry, and (*6*) stirring blade. **b** Holding method and orientation of specimen

Table 1 Parameters for the erosion–corrosion test used in this study

Slurry composition	20 wt% Al_2O_3 particles + 3.5% NaCl solution
Particle size range (μm)	S: 255–335, L: 530–625
Impact velocity (m/s)	4.2, 7.3, 10.4
Impact angle (°)	15, 30, 45, 60, 75, 90
Test duration (min)	120
Test temperature (°C)	20

The wear surface morphology was observed using the scanning electron microscope (SEM) of JEOL JSM-5600 in order to study the mechanism of erosion–corrosion wear of NAK80 mold steel in erosion–corrosion wear tests.

To analyze the synergism between erosion and corrosion, some weight loss tests in distilled water with 20 wt% Al_2O_3 particles were also conducted to obtain the pure erosion rates (W_e).

Results and discussion

Morphology

Study of the erosion–corrosion wear mechanisms of NAK80 mold steel by SEM revealed that the steel has been removed by a gradual pitting process. As the specimens expose to slurry, the oxide film first develops to inhibit the uniform corrosion. This passivation oxide film might be broken or removed to form anodic regions due to the repeated impingement and, then, pitting corrosion forms from breakdown sites of the passivation film. In order to investigate the development of the erosion–corrosion pits, the eroded surface was observed after testing at 5, 10, 15, 20, 25, and 30 min, respectively. Typical surface features after impingement with small particles at 30° impact angle and 7.3 m/s impact velocity are shown in Fig. 3. In Fig. 3a, some circular pits appear on the surface after impingement for 5 min, because the passivating oxide film has been damaged mechanically. Rupture of the oxide film causes rapid anodic reaction of the metal. The eroded surface after 10-min impingement is shown in Fig. 3b, which clearly indicates more pits, measured by image analysis, than that after 5-min impingement due to the formation of new pits. The size and dimension of pits were found to increase. After 15-min impingement, a large amount of corrosion products were found to agglomerate within and next to the pit area, as shown in Fig. 3c. These agglomerated corrosion products cover the scar area, and a scar trailing along the direction of particle motion is observed. In this case, numerous particles impacted on the surface deforming the surface plastic repeatedly, producing the fatigue cracks. Hence, the crack linkages near the existing pits are clearly

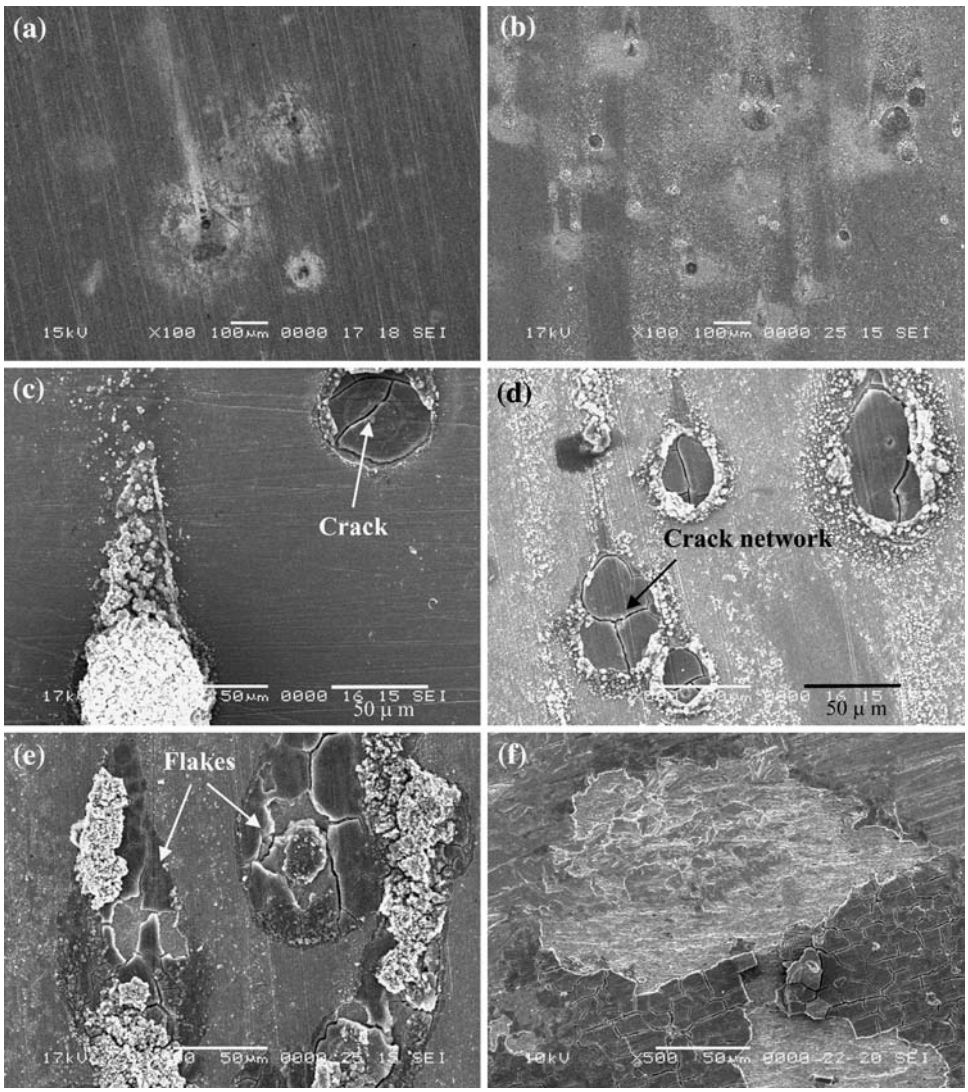

Fig. 3 The evolution of the erosion–corrosion on the NAK80 mold steel surface at 30° impact angle and an impact velocity of 7.3 m/s with small particles: **a** after 5 min, **b** after 10 min, **c** after 15 min, **d** after 20 min, **e** after 25 min, and **f** after 30 min

shown. As the impingement progresses to 20 min, loose corrosion products within many of pit areas might fall out, as shown in Fig. 3d. Meanwhile, the fatigue cracks propagated and interlaced with each other. As a result, surface crack networks are observed on the worn surface. In a corrosive environment, the galvanic cells might be responsible for the crack propagation that enhances the formation of surface crack networks on the worn surface. The cracks were acting as anode and the matrix was acting as cathode. Figure 3e shows the eroded surface after 25-min impingement. When flakes are formed, the contact area between flake and substrate decreases during the subsequent impingements due to delamination. Consequently, flakes within many of the pit areas might fall out partly, which in turn increases the erosion–corrosion rate (W_t). After 30 min, the size of some pits increases significantly and they are irregularly shaped; the flakes within the pit area fall out completely and the fresh metal is revealed. At this point, the cracks are distributed not only in the pits, but also over the surface of NAK80 mold steel, as shown in Fig. 3f.

The morphology of eroded surface depends strongly on the impact angle, impact velocity, and particle size. Figure 4 shows the surface features after 30-min impingement with small particles at six different impact angles at a constant velocity of 10.4 m/s. As shown in Fig. 4, the length of the scar trails progressively decreases with an increase in impact angle from 30° to 90° due to a decrease in the resolved shear stress. In contrast, the depth of the pits progressively increases with the impact angle because of an increase in the resolved normal stress. However, the particle at oblique angle tends to scratch the specimen surface rather than indent, resulting in a larger scar area that extends along the direction of impingement. Hence, the scar areas at impact angles of 30° and 45° are larger than those at other impact angles, and this increase in scar area could possibly lead to an increase in the erosion–corrosion rate because pitting occurs preferentially along

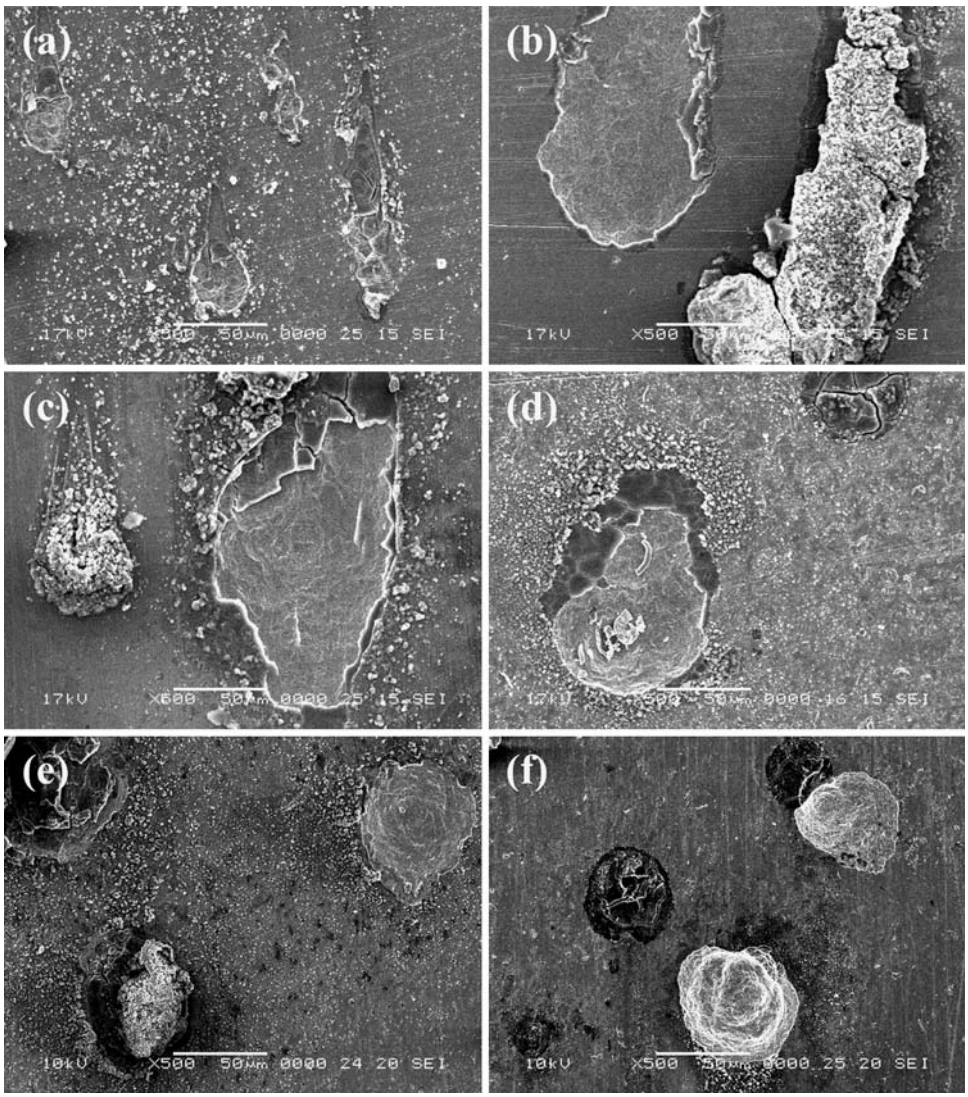

Fig. 4 The erosion–corrosion surface features after 30-min impingement with small particles at six different impact angles and at a constant velocity of 10.4 m/s: **a** 15°, **b** 30°, **c** 45°, **d** 60°, **e** 75°, and **f** 90°

the scratch [25]. Moreover, the corrosion products tend to be removed at high-impact angles. When the particle impingement angle is between 15° and 45°, the cutting mechanism mainly covers the impact pits and is the main mechanism of degradation, whereas at impact angles between 60° and 90°, the flakes within the impact pit area directly fall out due to plastic deformation fatigue spalling or cracking. Additionally, the morphology of eroded surfaces after impingement under other impact velocities (4.2 and 7.3 m/s) or/and large particle is similar to that shown in Fig. 4. However, both the pit depth and scar area significantly increase with the impact velocity and particle size.

Weight loss data

The polarization curve for NAK80 mold steel is shown in Fig. 5. It does not show any passivation and undergoes continuous dissolution, and the corrosion potential is −0.50 V (SCE). A corrosion current of 1 mA/cm^2 is equal to a weight loss of 1.04 mg/cm^2 h according to Faraday's law, assuming a density of 7.8 g/cm^3 and the atomic weight of iron as 55.85 for NAK80 mold steel. According to the polarization curve, the corrosion current is 0.016 mA/cm^2 and the corresponding pure corrosion rate is 0.017 mg/cm^2 h.

Figure 6 shows the variation in the pure erosion rate with impact angle for different impact velocities and particle sizes. The results shown in Fig. 6a, b agree with our common knowledge; it shows typical ductile erosion behavior. The pure erosion rate first increases and then decreases with the impact angles increasing from 15° to 90° with a maximum of around 30°. At a given impact angle, the pure erosion rate also increases with the impact velocity and particle size. A typical worn surface of erosion after 30-min impingement with small particles at 30° impact angle and a constant velocity of 10.4 m/s is shown in Fig. 7. Compared to the worn surface of the erosion–corrosion specimen impinged with the same condition

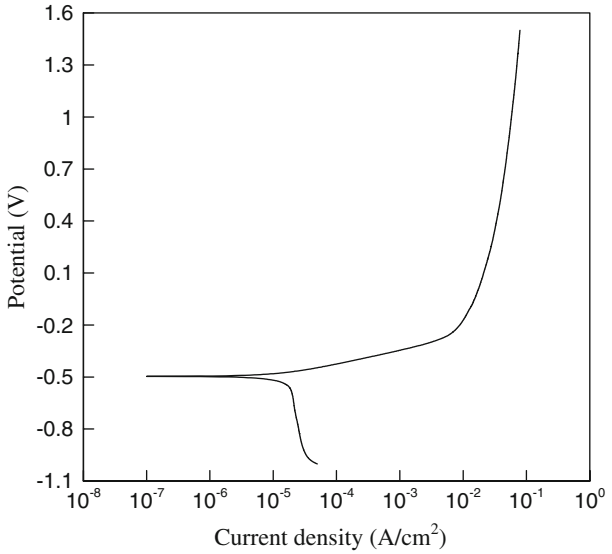

Fig. 5 Polarization curves of NAK80 mold steel in 3.5% NaCl solution

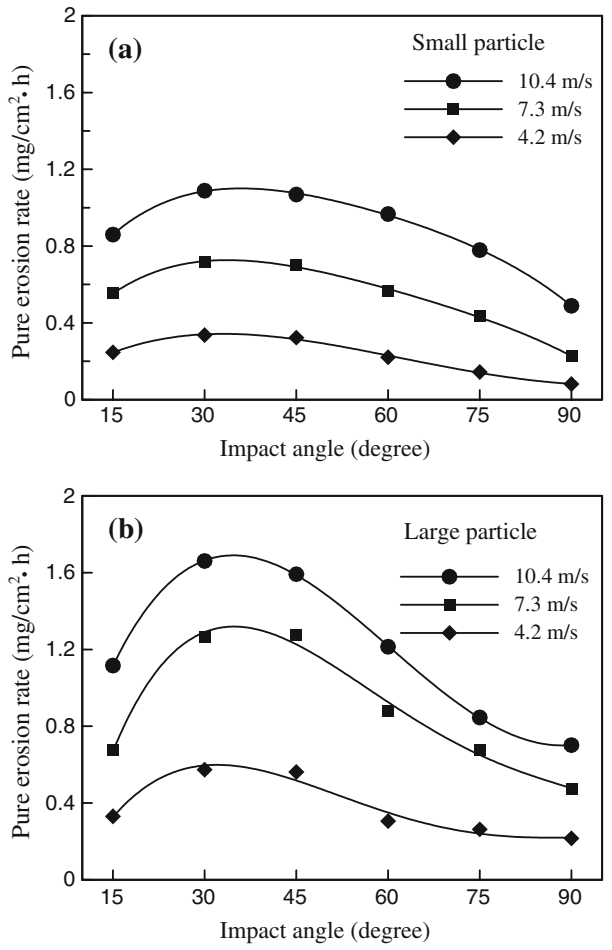

Fig. 6 Pure erosion rate plotted as a function of impact angle for different impact velocities and particle sizes: **a** small particle and **b** large particle

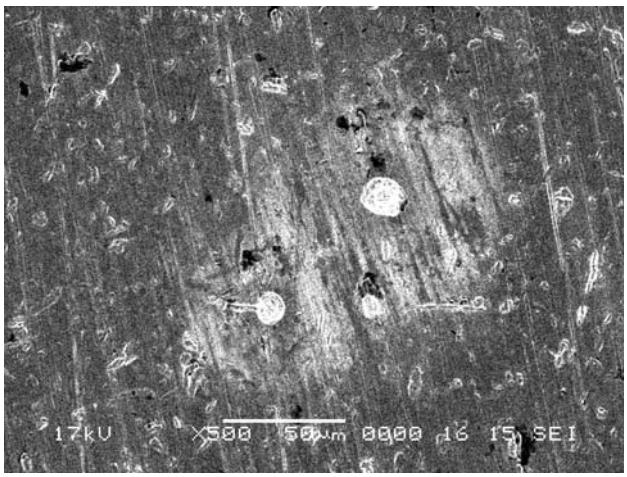

Fig. 7 Worn surface of erosion after 30-min impingement with small particles at 30° impact angle and a constant velocity of 10.4 m/s

(Fig. 4a), the surface reveals obvious erosion attacks and slight corrosion tracks. The pit size is smaller and the corrosion products are not noticeable. This feature indicates that the NAK80 mold steel would be corroded in distilled water. However, the weight loss is mainly caused by erosion.

The effect of the surface roughness on the erosion–corrosion rate of the specimens impinged with small particles at 30° impact angle and a constant velocity of 4.2 m/s was measured. Figure 8 shows the results of three experiments for different initial surface finishes as a function of time of slurry impingement. The effects are clear. Initially, after 10-min impingement, a rougher surface has a higher erosion–corrosion rate, but this difference decreases with increasing time of impingement. All surfaces showed almost the same erosion–corrosion rate after 60-min impingement. This demonstrates that the effect of the original roughness had been obliterated by impact of the slurry

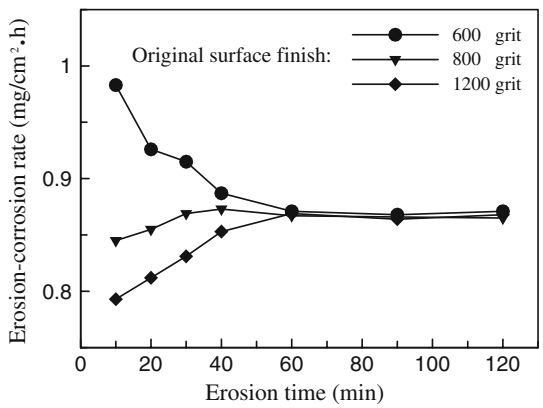

Fig. 8 Erosion–corrosion rate plotted as a function of erosion time for different initial surface finishes using small particles at an impact angle of 30° and a constant velocity of 4.2 m/s

when the erosion time exceeds 60 min. In our experiment, the duration of erosion–corrosion test is 120 min. Therefore, the effect of initial surface roughness on the erosion–corrosion rate is negligible.

Figure 9 shows the erosion–corrosion rate of the tested steel as a function of impact angle for different impact velocities and particle sizes. There is evidence that the erosion–corrosion rate increases with impact velocity and particle size at all impact angles. This characteristic is different from the results obtained by Lopez et al. [22]. They indicated that a decrease in the erosion–corrosion rate was observed for normal incidence when the impact velocity increased from 6.9 to 8.5 m/s, because the basic mechanism leading to mass loss was the ductile fracture of flakes formed on the eroded surface (see Figs. 7 and 8 of Ref. [22]). However, in our case, the flakes were directly removed by cracking or fatigue spalling induced by stress and corrosion for normal incidence. Therefore, the erosion–corrosion rate increases with the impact velocity and particle size because the impact energy is higher. Nevertheless, all the maximum peaks of erosion–corrosion rate are not at an impact angle of 30°, as shown in Fig. 9. They shift to higher impact angles of 45°. These differences indicate that the erosion–corrosion rate depends on pure corrosion, pure erosion, and more importantly the synergistic effects between erosion and corrosion in which the wear mechanism possibly changes; this will be further discussed below.

Synergistic effect

The synergistic weight loss rate (W_s) is calculated by using the following equation [6, 8, 10].

$$W_s = W_t - W_e - W_c \quad (1)$$

Figure 10 shows the synergistic weight loss rate as a function of impact angle for different impact velocities and particle sizes. For all three impact velocities and two particle sizes, the synergistic weight loss rates increase with decreasing impact angle but starts to considerably decrease after 45°.

At oblique angles between 30° and 45°, cutting becomes the major mechanism of slurry erosion. In this case, the passive film and the flakes are scraped off instead of braking or rupturing. As a result, a larger denuded area is

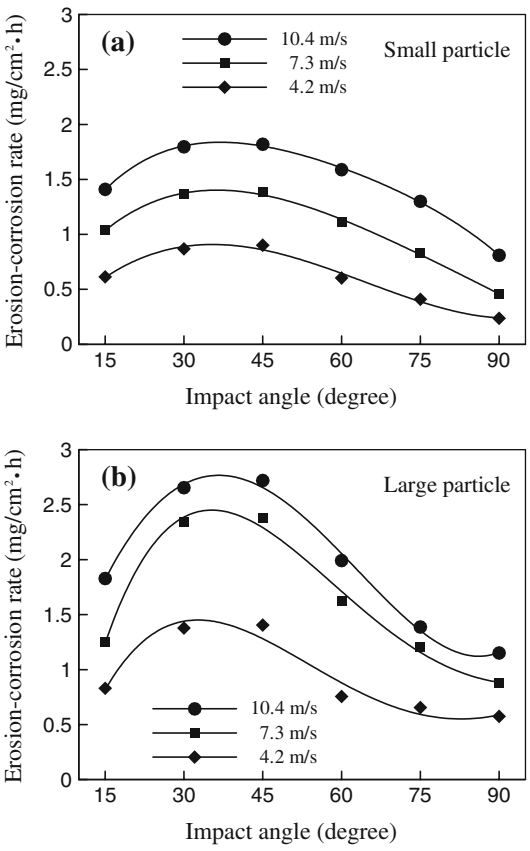

Fig. 9 Erosion–corrosion rate plotted as a function of impact angle for different impact velocities and particle sizes: **a** small particle and **b** large particle

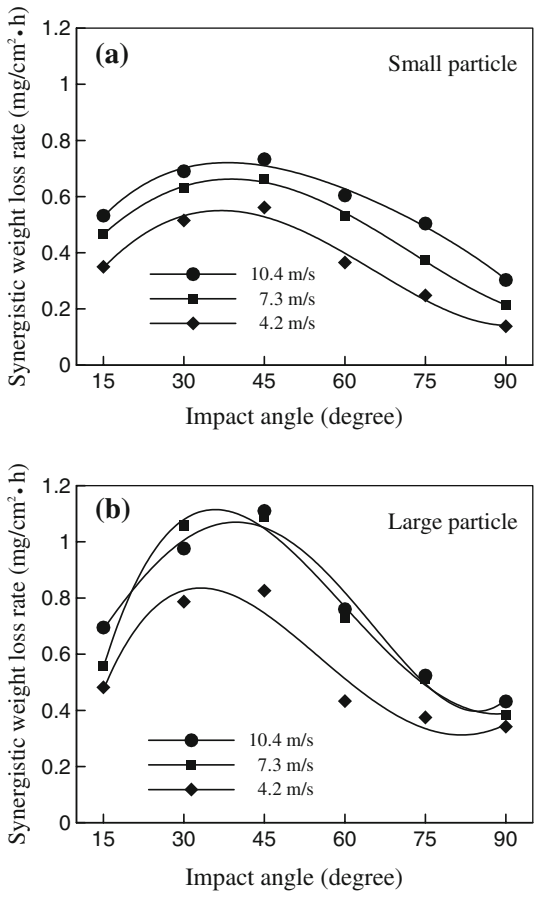

Fig. 10 Synergistic weight loss plotted as a function of impact angle for different impact velocities and particle sizes: **a** small particle and **b** large particle

generated, thereby leading to the enhancement of erosion-enhanced corrosion by dissolution of metallic matrix. In addition, the scar area and amount of flakes are larger at the impact angles of 30° and 45° than at those other impact angles (Fig. 4a, b). The load-bearing area of the flake is the site of deleterious localized corrosion as it is occluded. Thus, pitting occurs at the load-bearing area, and it accelerates the detachment of the flakes. Even though pits may repassivate before the flake detaches, subsequent particle impacts may lead to the detachment more readily. This mechanism comprises corrosion-enhanced erosion. As a result, the maximum synergistic weight loss rates are obtained between 30° and 45°.

At high-impact angles (60°–90°), the magnitude of the synergistic effect is lower. This is due to three reasons. First, the particle striking at higher impact angles indents or deforms the metal surface rather than cutting it, and the broken or ruptured passive film may remain adherent on the scar. Second, a small scar area is generated by particle impingement at more normal angles, as shown in Fig. 4d–f. Because of these two effects, indentation of the true bare-metal area is smaller than that in cutting, thereby lowering the erosion-enhanced corrosion. Third, the amount of the fallen out flakes at higher impact angles is also smaller than that at oblique angles, indicating that corrosion-enhanced erosion is insignificant. Consequently, the synergistic weight loss rates at higher impact angles are smaller than those at oblique angles.

At the highest oblique angle (15°), the scars become shallower and extend more in the direction of particle motion, thereby resulting in a smaller pit area (Fig. 4a) than that developed on the surfaces eroded at 30° and 45° (Fig. 4b, c). A pitted metal surface is vulnerable to material removal by subsequent particle impact because the generation of pits locally weakens the material surface. As less pit area is formed, the corrosion-enhanced erosion decreases; the synergism, thus, becomes smaller than that of the erosion at impact angles of 30° and 45°.

Figure 10 also shows that the synergistic weight loss rate is greater at higher impact velocities and for large particles at a given impact angle. It is possible that with the increases in impact velocity and particle size, rupture of the oxide film increases due to the higher impact energy, thereby leading to an enhancement in the corrosion rate. Higher impact velocities and large particles also tend to remove the corrosion products and develop a larger scar area. As a result, there is an increase in the rate of synergistic weight loss.

On the basis of the experimental results, it is proposed that the main mechanisms of erosion–corrosion identified in NAK80 mold steel at high-impact angles are the formation of impact pits, dissolution of metallic matrix, and plastic deformation fatigue spalling (Fig. 11a), whereas at low-impact angles, the mechanisms are dominated by the formation of impact pits, dissolution of metallic matrix, fatigue cracks, and cutting (Fig. 11b).

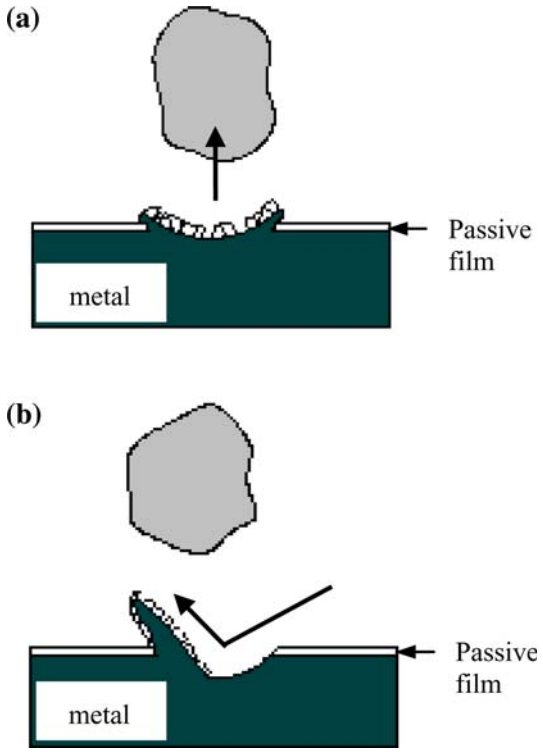

Fig. 11 Schematic diagrams showing the erosion–corrosion mode of the worn surfaces for **a** high- and **b** low-impact angle

To illustrate how different parameters influence the contribution of synergism on the total weight loss (W_s/W_t) more clearly, the variation in W_s/W_t with the impact angles for three different impact velocities and two different particle sizes is shown in Fig. 12. These results indicate that the synergistic effect is 40–60% of the total weight loss. The values of W_s/W_t depend upon the impact velocity, but are almost independent of the impact angle and particle size. The contribution of synergism is higher at low velocity than that at high velocity because the pure erosion component decreases with a decrease in the impact velocity.

Conclusions

In this investigation, the erosion–corrosion behavior of NAK80 mold steel has been examined over the range of conditions. The main conclusions from this investigation can be summarized as follows:

1. The erosion–corrosion mechanisms of NAK80 mold steel at high-impact angles are formation of impact pits, dissolution of metallic matrix, and plastic

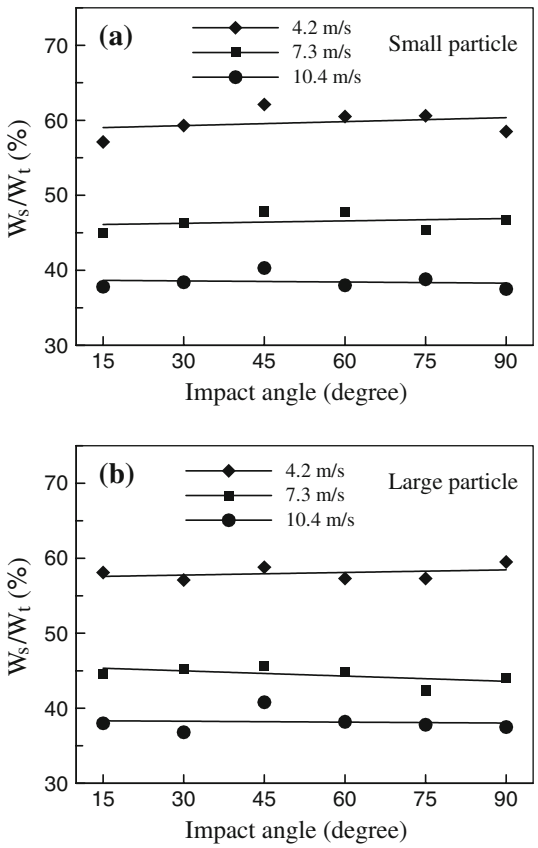

Fig. 12 Ratio of W_s/W_t plotted as a function of impact angle for different impact velocities and particle sizes: **a** small particle and **b** large particle

deformation fatigue spalling, whereas at low-impact angles, the mechanisms are dominated by the formation of impact pits, dissolution of metallic matrix, fatigue cracks, and cutting. The observed synergism between these mechanisms is much more accentuated at oblique impact angles than at normal impact angles.

2. Weight loss measurements demonstrate that the overall material loss and its pure erosion component are significantly affected by the impact angle, impact velocity, and particle size. The maximum peak of erosion rates lies at oblique angles between 30° and 45°, whereas the maximum of the erosion–corrosion rates appears at 45°, and the erosion–corrosion rate is higher than the erosion rate alone at all angles examined, thereby indicating a positive synergism between erosion and corrosion for NAK80 mold steel in solid/aqueous slurry. At a given impact angle, the erosion–corrosion rate would increase with the impact velocity and size of solid particles.
3. The synergistic effect is 40–60% of the total weight loss. The contribution of synergism on the total weight loss depends upon the impact velocity, but it is almost independent of the impact angle and particle size. This contribution increases with a decrease in the impact velocity.

References

1. http://www.daido.co.jp/english/products/tool/plasticmold.html. Accessed 15 June 2009
2. Sheir LL, Jarman RA, Burstein GT (1994) Corrosion, corrosion control. Butterworth-Heinemann, Oxford
3. Zu JB, Hutchings IM, Burstein GT (1990) Wear 140:331
4. Matsumura M, Oka Y, Hiura H, Yano M (1991) ISIJ Int 31:168
5. Lopez D, Falleiros NA, Tschiptschin AP (2007) Wear 263:347
6. Stack MM, Pungwiwat N (2004) Wear 256:565
7. Li XY, Yan YG, Ma L, Xu ZM, Li JG (2004) Mater Sci Eng A 382:82
8. Guo HX, Lu BT, Luo JL (2005) Electrochim Acta 51:315
9. Guenbour A, Hajji MA, Jallouli EM, Bachir AB (2006) Appl Surf Sci 253:2362
10. Meng H, Hu X, Neville A (2007) Wear 263:355
11. Zheng YG, Yu H, Jiang SL, Yao ZM (2008) Wear 264:1051
12. Zheng Y, Yao Z, Wei X, Ke W (1995) Wear 186–187:555
13. Nesic S, Postlethwaite J, Olsen S (1995) Corrosion 4:131
14. Liu ZY, Dong CF, Li XG, Zhi Q, Cheng YF (2009) J Mater Sci 44:4228. doi:10.1007/s10853-009-3520-x
15. Niu L, Yin YH, Guo WK, Lu M, Qin R, Chen S (2009) J Mater Sci 44:4511. doi:10.1007/s10853-009-3654-x
16. Kermani MB, Morshed A (2003) Corrosion 59:659
17. Chaudhary D, Liu HH (2009) J Mater Sci 44:4472. doi:10.1007/s10853-009-3678-2
18. Behpour M, Ghoreishi SM, Gandomi-Niasar A, Soltani N, Salavati-Niasari M (2009) J Mater Sci 44:2444. doi:10.1007/s10853-009-3309-y
19. Clark HM, Hartwich RB (2001) Wear 248:147
20. Burstein GT, Sasaki K (2000) Wear 240:80
21. Stack MM, Abd Ei Badia TM (2006) Surf Coat Technol 201:1335
22. Lopez D, Congote JP, Cano JR, Toro A, Tschiptschin AP (2005) Wear 259:118
23. Calliari I, Brunelli K, Zanellato M, Ramous E, Bertelli R (2009) J Mater Sci 44:3764. doi:10.1007/s10853-009-3505-9
24. Sasaki K, Burstein GT (1996) Corros Sci 38:2111
25. Burstein GT, Davies DH (1980) Corros Sci 20:1143